ICMERE2013-PI-043

NUMERICAL SOLUTION OF UNSTEADY MHD CHEMICALLY REACTING MICROPOLAR FLUID FLOW THROUGH A POROUS MEDIUM ALONG AN IMPULSIVE PERMEABLE VERTICAL PLATE

Mohammad Wahiduzzaman[1], Md. Mahmud Alam[2] and Tanvir Ahmed[3]

[1-3]Mathematics Discipline, Khulna University, Khulna-9208, Bangladesh

[1]wahidmathku@gmail.com, [2]alam_mahmud2000@yahoo.com, [3]tanvir1989bd@gmail.com

Abstract *- Unsteady MHD chemically reacting micropolar fluid over an impulsive vertical plate in porous media in the presence of internal heat generation and thermal radiation has been studied. To obtain the non-similar momentum, angular momentum, energy and concentration equations, usual non-dimensional variables have been used. The implicit finite difference technique with stability analysis is used to solve the non-similar, coupled, non linear partial differential non-dimensional equations. The obtained solutions have been shown graphically. Finally, a qualitative comparison with previous work is shown in tabular form.*

Keywords: Micropolar Fluid, Chemical Reaction, Implicit Finite Difference.

1. INTRODUCTION

The Micropolar fluids are fluids with microstructure belonging to a class of fluids with nonsymmetrical stress sensor referred to as polar fluids. Physically, they represent fluids consisting of randomly oriented particles suspended in a viscous medium, and they are important to engineers and scientists working with hydrodynamic-fluid problems and phenomena. The concept of micropolar fluid deals with a class of fluids that exhibit certain microscopic effects arising from the micromotions of the fluid elements. These fluids contain dilute suspension of rigid macromolecules with individual motions that support stress and body moments and are influenced by spin inertia. Micropolar fluids are those which contain micro-constituents that can undergo rotation, the presence of which can affect the hydrodynamics of the flow so that it can be distinctly non-Newtonian. It has many practical applications, for example, analyzing the behavior of exotic lubricants, the flow of colloidal suspensions or polymeric fluids, liquid crystals, additive suspensions, human and animal blood, turbulent shear flow and so forth.

The Joule heating effects on MHD free convection flow of a micropolar fluid have been investigated by El-Haikem et al. [1]. The MHD free convection and mass transfer flow in micropolar fluid with constant suction have been studied by El-Amin [2]. The MHD convective flow of a micropolar fluid past a continuously moving vertical porous plate in the presence of heat generation/absorption have been analyzed by Rahman and Sattar [3]. In the above mentioned papers, most of the previous works assume that the plate is at rest. The heat and mass transfer in MHD micrpoloar flow over a

vertical moving porous plate in a porous medium have been studied by Kim [4]. The effects of radiation, free convection and mass transfer on an unsteady flow of a micropolar fluid over a vertical moving porous plate immersed in a porous medium with time varying suction have been analyzed by Kumar et al. [5]. The Joule heating and thermal diffusion effects on unsteady MHD free convective heat and mass transfer flow of a micropolar fluid through a vertical infinite porous medium under the action of a transverse magnetic field taking into account a constant heat source with constant heat and mass fluxes have been investigated by Haque and Alam [6].

Hence our aim of this work is to extend the work of Haque and Alam [6] with chemical reaction effects. The problem has been solved by implicit finite difference method (Carnahan et al. [7]). The governing equations involved in this problem have been transformed into dimensionless non-similar coupled partial differential equation by usual transformations. Finally, the qualitative comparison of the present results with the results of Haque and Alam [6] has been shown.

2. MATHEMATICAL FORMULATIONS

The unsteady MHD mixed convective heat and mass transfer flow of an electrically conducting incompressible viscous fluid past an electrically nonconducting isothermal infinite permeable impulsive vertical plate with thermal diffusion and diffusion thermo effects have been considered. The effects of internal heat generation, joule heating, viscous dissipation and chemical reaction have been also considered. The positive x coordinate is measured

along the plate in the direction of fluid motion and the positive y coordinate is measured normal to the plate. Initially, it is considered that the plate as well as the fluid is at the same temperature $T(=T_\infty)$ and concentration level $C(=C_\infty)$. Also it is assumed that the fluid and the plate is at rest after that the plate is to be moving with a constant velocity U_∞ in its own plane. Instantaneously at time $t > 0$, the temperature of the plate and spices concentration are raised to $T_w(>T_\infty)$ and $C_w(>C_\infty)$ respectively, which are there after maintained constant, where T_w, C_w are temperature and spices concentration at the wall and T_∞, C_∞ are the temperature and concentration of the species outside the plate respectively. The physical configuration of the problem is furnished in Figure 1.
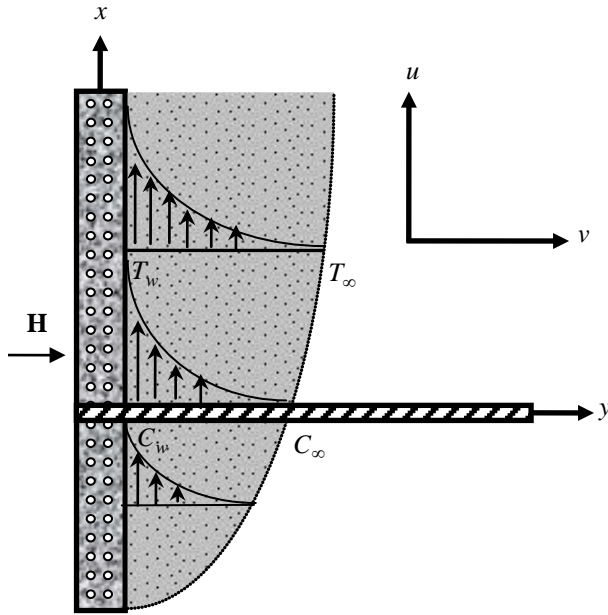

Fig 1: Physical configuration and coordinate system.

A strong uniform magnetic field **H** is imposed parallel to the y–axis and it can be taken as $(0, H_0, 0)$. The magnetic Reynolds number of the flow is taken to be small enough field and the magnetic field is negligible in comparison with applied magnetic field and the magnetic lines are fixed relative to the fluid. Using the relation $\nabla \cdot \mathbf{J} = 0$ for the current density $\mathbf{J} = (J_x, J_y, J_z)$ where $J_y = \text{constant}$. Since the plate is nonconducting, $J_y = 0$ at the plate and hence zero everywhere.

If the plate is infinite in extent and hence all physical quantities depend on y and t. Within the above framework of the above stated assumptions and using the dimensionless quantities,

$$Y = \frac{yU_\infty}{\upsilon} \quad , \quad U = \frac{u}{U_\infty} \quad , \quad \Gamma = \frac{\Omega \upsilon}{U_\infty^2} \quad , \quad \tau = \frac{tU_\infty^2}{\upsilon} \quad ,$$

$$\overline{T} = \frac{T - T_\infty}{T_w - T_\infty}, \ \overline{C} = \frac{C - C_\infty}{C_w - C_\infty} \ \text{ with parameters } \varepsilon = \frac{v_0}{U_\infty},$$

$$\Delta = \frac{\chi}{\rho \upsilon}, \ G_r = \frac{gB_T(T_w - T_\infty)\upsilon}{U_\infty^3}, \ G_m = \frac{gB_C(C_w - C_\infty)\upsilon}{U_\infty^3},$$

$$M = \frac{\sigma \mu_e^2 H_0^2 \upsilon}{\rho U_\infty^2}, \ \Lambda = \frac{\gamma}{\rho j \upsilon}, \ \lambda = \frac{\chi \upsilon}{\rho j U_\infty^2}, \ R = \frac{16\sigma^* T_\infty^3}{3k^* \kappa},$$

$$P_r = \frac{\rho c_p \upsilon}{\kappa} \quad , \qquad D_u = \frac{Dk_t}{\upsilon c_s c_p} \frac{(C_w - C_\infty)}{(T_w - T_\infty)} \quad ,$$

$$E_c = \frac{U_\infty^2}{c_p(T_w - T_\infty)} \quad , \quad \beta = \frac{Q\upsilon}{\rho c_p U_\infty^2} \quad , \quad S_c = \frac{\upsilon}{D} \quad ,$$

$$S_r = \frac{Dk_T}{\upsilon T_m} \frac{(T_w - T_\infty)}{(C_w - C_\infty)} \ \text{ as well as } \ \gamma = \frac{k_0 \upsilon}{U_\infty^2} \ \text{ the equations}$$

relevant to the unsteady two dimensional problem is governed by the following non-dimensional system of coupled nonlinear partial differential equations under the boundary layer approximations as;

$$\frac{\partial U}{\partial \tau} - \varepsilon \frac{\partial U}{\partial Y} = (1 + \Delta)\left(\frac{\partial^2 U}{\partial Y^2}\right) + \Delta \frac{\partial \Gamma}{\partial Y} + G_r \overline{T}$$
$$+ G_r \overline{C} - MU \qquad (1)$$

$$\frac{\partial \Gamma}{\partial T} - \varepsilon \frac{\partial \Gamma}{\partial Y} = \Lambda \left(\frac{\partial^2 \Gamma}{\partial Y^2}\right) - \lambda \left(2\Gamma + \frac{\partial U}{\partial Y}\right) \qquad (2)$$

$$\frac{\partial \overline{T}}{\partial \tau} - \varepsilon \frac{\partial T}{\partial Y} = \left(\frac{1 + R}{P_r}\right)\frac{\partial^2 \overline{T}}{\partial Y^2} + D_u \frac{\partial^2 \overline{C}}{\partial Y^2} + E_c(1 + \Delta)\left(\frac{\partial U}{\partial Y}\right)^2$$
$$+ ME_c U^2 + \beta \overline{T} \qquad (3)$$

$$\frac{\partial \overline{C}}{\partial \tau} - \varepsilon \frac{\partial \overline{C}}{\partial Y} = \frac{1}{S_c}\frac{\partial^2 \overline{C}}{\partial Y^2} + S_r \frac{\partial^2 \overline{T}}{\partial Y^2} - \gamma \overline{C} \qquad (4)$$

with the corresponding boundary conditions are;

$$U = 1, \ \Gamma = -S\frac{\partial U}{\partial Y}, \ \overline{T} = 1, \ \overline{C} = 1 \ \text{at } Y = 0 \qquad (5)$$

$$U = 0, \ \Gamma = 0, \ \overline{T} = 0, \ \overline{C} = 0 \ \text{as } Y \rightarrow \infty,$$

3. SHEAR STRESS, COUPLE STRESS, NUSSELT AND SHERWOOD NUMBER

From the velocity field, the effects of various parameters on the shear stress have been calculated. The following equation represents the shear stress at the plate, the shear stress, $\tau_x = \left[\mu_0 + (1 - S)\chi\right]\left(\frac{\partial U}{\partial Y}\right)_{Y=0}$ which is proportional to $\left(\frac{\partial U}{\partial Y}\right)_{Y=0}$. From the angular velocity field, the effects of various parameters on the couple stress have been analyzed. The following equation represents the couple stress at the wall, $M_x = \frac{\upsilon j \rho}{\gamma}\left(\frac{\partial \Gamma}{\partial Y}\right)_{Y=0}$ which is proportional to $\left(\frac{\partial \Gamma}{\partial Y}\right)_{Y=0}$. From the temperature field, the effects of various parameters on the heat transfer coefficients have been analyzed. The following equation represents the heat transfer rate that is well known Nusselt number, the Nusselt number, $N_u = -\mu_0\left(\frac{\partial T}{\partial y}\right)_{y=0}$ which is

proportional to $-\left(\dfrac{\partial \overline{T}}{\partial Y}\right)_{Y=0}$. And from the concentration field, the effects of various parameters on the mass transfer coefficients have been studied. The following equation represents mass transfer rate that is well known Sherwood number, the Sherwood number,

$$S_h = -\mu_0 \left(\frac{\partial C}{\partial y}\right)_{y=0}$$ which is proportional to

$$-\left(\frac{\partial \overline{C}}{\partial Y}\right)_{Y=0}.$$

4. NUMERICAL SOLUTIONS

To solve the non-dimensional system by the implicit finite difference technique, it is required a set of finite difference equations. In this case, the region within the boundary layer is divided by some perpendicular lines of Y-axis, where Y-axis is normal to the medium as shown in Figure 2. It has been assumed that the maximum length of boundary layer is $Y_{\max} = (10)$ as corresponds to $Y \to \infty$ i.e. Y varies from 0 to 10 and the number of grid spacing in Y directions is $\overline{p}(=100)$, hence the constant mesh size along Y axis becomes $\Delta Y = 0.10\,(0 \le Y \le 10)$ with a smaller time-step $\Delta \tau = 0.001$.
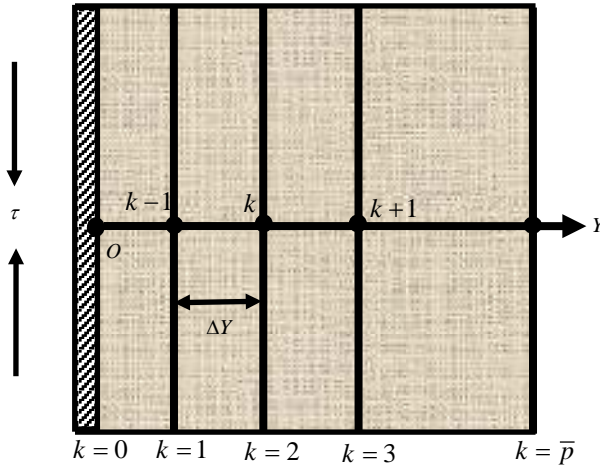

Fig.2: Implicit finite difference system grid.

Let $U^{\overline{n}}$, $\Gamma^{\overline{n}}$, $\overline{T}^{\overline{n}}$ and $\overline{C}^{\overline{n}}$ denote the values of $U, \Gamma, \overline{T}$ and $\overline{C}$ at the end of a time-step respectively. Using the implicit finite difference approximation, the following appropriate set of finite difference equations are obtained as;

$$\frac{U_k^{\overline{n}+1} - U_k^{\overline{n}}}{\Delta \tau} - \varepsilon \frac{U_{k+1}^{\overline{n}} - U_k^{\overline{n}}}{\Delta Y} = (I + \Delta)\frac{U_{k+1}^{\overline{n}} - 2U_k^{\overline{n}} + U_{k-1}^{\overline{n}}}{(\Delta Y)^2}$$

$$+ \Delta \frac{\Gamma_{k+1}^{\overline{n}} - \Gamma_k^{\overline{n}}}{\Delta Y} + G_r \overline{T}_k^{\overline{n}} + G_m \overline{C}_k^{\overline{n}} - MU_k^{\overline{n}} \quad (6)$$

$$\frac{\Gamma_k^{\overline{n}+1} - \Gamma_k^{\overline{n}}}{\Delta \tau} - \varepsilon \frac{\Gamma_{k+1}^{\overline{n}} - \Gamma_k^{\overline{n}}}{\Delta Y} = \Lambda \frac{\Gamma_{k+1}^{\overline{n}} - 2\Gamma_k^{\overline{n}} + \Gamma_{k-1}^{\overline{n}}}{(\Delta Y)^2}$$

$$- \lambda \left(2\Gamma_k^{\overline{n}} + \frac{U_{k+1}^{\overline{n}} - U_k^{\overline{n}}}{\Delta Y}\right) \quad (7)$$

$$\frac{\overline{T}_k^{\overline{n}+1} - \overline{T}_k^{\overline{n}}}{\Delta \tau} - \varepsilon \frac{\overline{T}_{k+1}^{\overline{n}} - \overline{T}_k^{\overline{n}}}{\Delta Y} = \left(\frac{1+R}{P_r}\right)\frac{\overline{T}_{k+1}^{\overline{n}} - 2\overline{T}_{ki}^{\overline{n}} + \overline{T}_{k-1}^{\overline{n}}}{(\Delta Y)^2}$$

$$+ D_u \frac{\overline{C}_{k+1}^{\overline{n}} - 2\overline{C}_k^{\overline{n}} + \overline{C}_{k-1}^{\overline{n}}}{(\Delta Y)^2} + E_c(I + \Delta)\left(\frac{U_{k+1}^{\overline{n}} - U_k^{\overline{n}}}{\Delta Y}\right)^2$$

$$+ ME_c\left(U_k^{\overline{n}}\right)^2 + \beta\left(\overline{T}_k^{\overline{n}}\right) \quad (8)$$

$$\frac{\overline{C}_k^{\overline{n}+1} - \overline{C}_k^{\overline{n}}}{\Delta \tau} - \varepsilon \frac{\overline{C}_{k+1}^{\overline{n}} - \overline{C}_k^{\overline{n}}}{\Delta Y} = \frac{1}{S_c}\frac{\overline{C}_{k+1}^{\overline{n}} - 2\overline{C}_k^{\overline{n}} + \overline{C}_{k-1}^{\overline{n}}}{(\Delta Y)^2}$$

$$+ S_r \frac{\overline{T}_{k+1}^{\overline{n}} - 2\overline{T}_k^{\overline{n}} + \overline{T}_{k-1}^{\overline{n}}}{(\Delta Y)^2} - \gamma\left(\overline{C}_k^{\overline{n}}\right) \quad (9)$$

with the boundary conditions,

$$U_0^{\overline{n}} = 1, \ \Gamma_k^{\overline{n}} = -S\frac{U_{k+1}^{\overline{n}} - U_k^{\overline{n}}}{\Delta Y}, \ \overline{T}_0^{\overline{n}} = 1, \ \overline{C}_0^{\overline{n}} = 1 \quad (10)$$

$$U_L^{\overline{n}} = 0, \ \Gamma_k^{\overline{n}} = 0, \ \overline{T}_L^{\overline{n}} = 0, \ \overline{C}_L^{\overline{n}} = 0 \ \text{ where } L \to \infty$$

Here the subscript k designates the grid points with Y coordinate and the superscript $\overline{n}$ represents a value of time, $\tau = \overline{n}\Delta \tau$ where $\overline{n} = 0,1,2,\ldots\ldots$. The velocity (U), angular velocity (Γ), temperature $(\overline{T})$ and concentration $(\overline{C})$ distributions at all interior nodal points may be computed by successive applications of the above finite difference equations. The numerical values of the shear stresses, Nusselt number and Sherwood number are evaluated by **Five-point** approximate formula for the derivatives. The stability conditions are

$$M\frac{\Delta \tau}{2} + S\frac{\Delta \tau}{\Delta Y} + \frac{2\Delta \tau}{(\Delta Y)^2} \le 1, \ S\frac{\Delta \tau}{\Delta Y} + \Lambda\frac{2\Delta \tau}{(\Delta Y)^2} + \lambda\Delta \tau \le 1,$$

$$-\beta\frac{\Delta \tau}{2} + S\frac{\Delta \tau}{\Delta Y} + \left(\frac{1+R}{P_r}\right)\frac{2\Delta \tau}{(\Delta Y)^2} \le 1 \qquad \text{and}$$

$$\gamma\frac{\Delta \tau}{2} + S\frac{\Delta \tau}{\Delta Y} + \frac{1}{S_c}\frac{2\Delta \tau}{(\Delta Y)^2} \le 1.$$ When the $\Delta \tau$ and ΔY approach to zero then the problem will be converged. That's mean the results of the implicit finite difference method approach the true solutions.

5. RESULTS AND DISCUSSION

To investigate the physical situation of the problem, the numerical results and graphs of dimensionless velocity (U), angular velocity (Γ), temperature $(\overline{T})$ and concentration $(\overline{C})$ within the boundary layer have been computed for different values of ε, Δ, G_r, M, Λ, λ, R, P_r, D_u, E_c, β, S_c, S_r and γ with the help of a computer programming language Compaq Visual Fortran 6.6a. Using Tecplot 7 these computed numerical results have been shown graphically. To obtain the steady-state solutions, the computations have been carried out up to dimensionless time, $\tau = 80$. It is observed that the numerical values of U, Γ, $\overline{T}$ and $\overline{C}$ however, show little changes after $\tau = 20$. Hence at $\tau = 20$ the solutions of all variables are steady-state solutions.

To observe the physical situation of the problem, the shear stress, couple stress, Nusselt number and Sherwood number have been illustrated in figures 3-13. The effects of various values of Suction parameter (ε), Grashof number (G_r), Magnetic parameter (M), Soret number (S_r), Microrotational number $(\varDelta)$ and Eckert number (E_c) on shear stress in case of cooling plate are presented in figures 3-5 respectively. It is observed that the shear stress increases with the increase of Grashof number and Soret number while decreases with the increase Suction parameter and Magnetic parameter.

Fig.3: Shear stress for ε, where $G_r = 1.00$, $G_m = 1.00$, $M = 1.00$, $\varDelta = 2.00$, $\varLambda = 2.00$, $\lambda = 0.50$, $R = 0.15$, $P_r = 0.71$, $D_u = 0.20$, $E_c = 0.50$, $\beta = 0.50$, $S_c = 0.60$, $S_r = 0.20$, $\gamma = 1.00$ and $S = 0.50$.
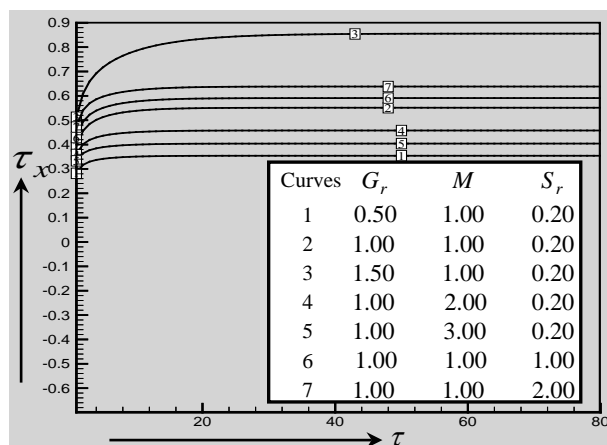

Curves	G_r	M	S_r
1	0.50	1.00	0.20
2	1.00	1.00	0.20
3	1.50	1.00	0.20
4	1.00	2.00	0.20
5	1.00	3.00	0.20
6	1.00	1.00	1.00
7	1.00	1.00	2.00

Fig.4: Shear stress for G_r, M and S_r, where $\varepsilon = 2.00$, $G_m = 1.00$, $\varDelta = 2.00$, $\varLambda = 2.00$, $\lambda = 0.50$, $R = 0.15$, $P_r = 0.71$, $D_u = 0.20$, $E_c = 0.50$, $\beta = 0.50$, $S_c = 0.60$, $\gamma = 1.00$ and $S = 0.50$.

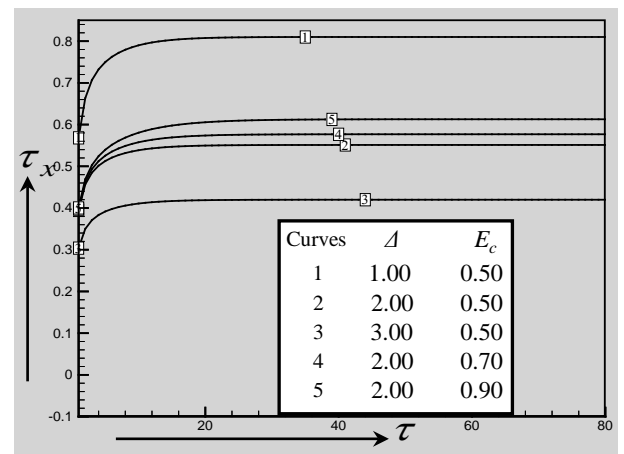| Curves	$\varDelta$	E_c
1	1.00	0.50
2	2.00	0.50
3	3.00	0.50
4	2.00	0.70
5	2.00	0.90

Fig.5: Shear stress for $\varDelta$ and E_c, where $\varepsilon = 2.00$, $G_r = 1.00$, $G_m = 1.00$, $M = 1.00$, $\varLambda = 2.00$, $\lambda = 0.50$, $R = 0.15$, $P_r = 0.71$, $D_u = 0.20$, $\beta = 0.50$, $S_c = 0.60$, $S_r = 0.20$, $\gamma = 1.00$ and $S = 0.50$.

In figures 6 and 7 display the effects of various values of Suction parameter (ε), Spin gradient viscosity $(\varDelta)$ and Vortex viscosity (λ) on couple stress have been shown respectively. These results show that the couple stress increases with the increase of Spin gradient viscosity while decreases with the increase Suction parameter and Vortex viscosity.
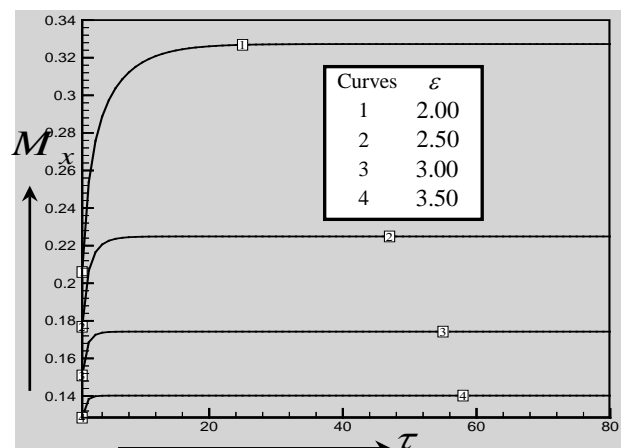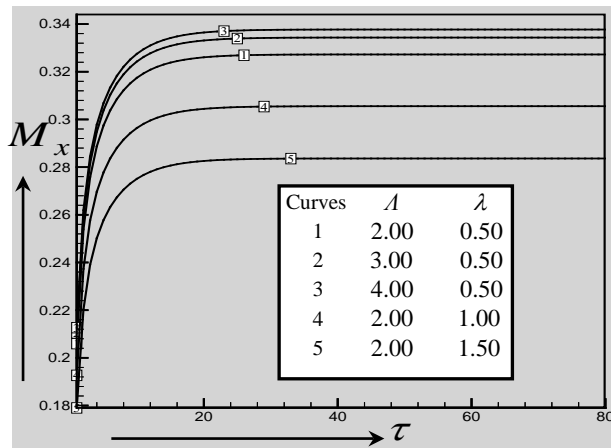

Curves	ε
1	2.00
2	2.50
3	3.00
4	3.50

Fig.6: Couple stress for ε, where $G_r = 1.00$, $G_m = 1.00$, $M = 1.00$, $\varDelta = 2.00$, $\varLambda = 2.00$, $\lambda = 0.50$, $R = 0.15$, $P_r = 0.71$, $D_u = 0.20$, $E_c = 0.50$, $\beta = 0.50$, $S_c = 0.60$, $S_r = 0.20$, $\gamma = 1.00$ and $S = 0.50$.

Fig.7: Couple stress for $\varLambda$ and λ, where $\varepsilon = 2.00$, $G_r = 1.00$, $G_m = 1.00$, $M = 1.00$, $\varDelta = 2.00$, $R = 0.15$, $P_r = 0.71$, $D_u = 0.20$, $E_c = 0.50$, $\beta = 0.50$, $S_c = 0.60$, $S_r = 0.20$, $\gamma = 1.00$ and $S = 0.50$.

In figures 8-12 display the Nusselt number for various values of Suction parameter (ε), Microrotational number $(\varDelta)$ Eckert number (E_c), Radiation parameter (R), Dufour number (D_u), Prandtl number (P_r) and Heat generation or absorption parameter (β) respectively. It is noted that $\beta < 0$ and $\beta > 0$ are treated as heat absorption and genaration respectively. These results show that the Nusselt number increases with the increase of Suction parameter, Microrotational number and Prandtl numbver while decreases with the increase of Eckert number, Radiation parameter, Dufour number and Heat generation or absorption parameter.
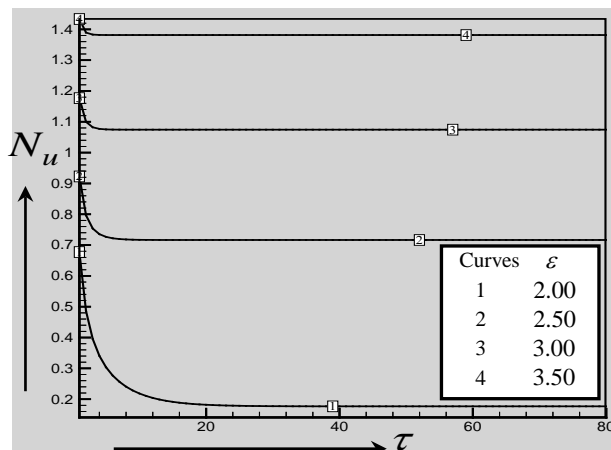

Fig.8: Nusselt number for ε, where $G_r = 1.00$, $G_m = 1.00$, $M = 1.00$, $\varDelta = 2.00$, $\varLambda = 2.00$, $\lambda = 0.50$, $R = 0.15$, $P_r = 0.71$, $D_u = 0.20$, $E_c = 0.50$, $\beta = 0.50$, $S_c = 0.60$, $S_r = 0.20$, $\gamma = 1.00$ and $S = 0.50$.
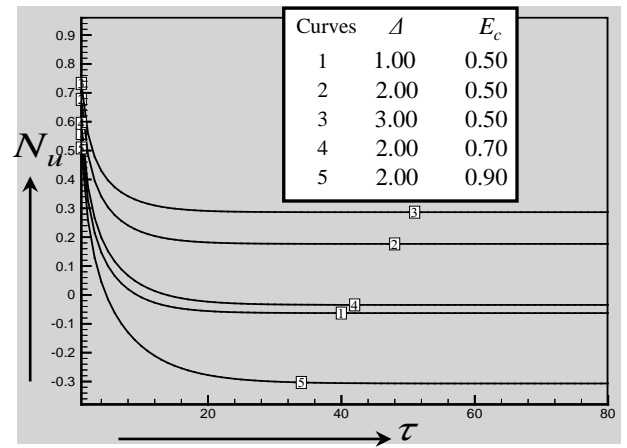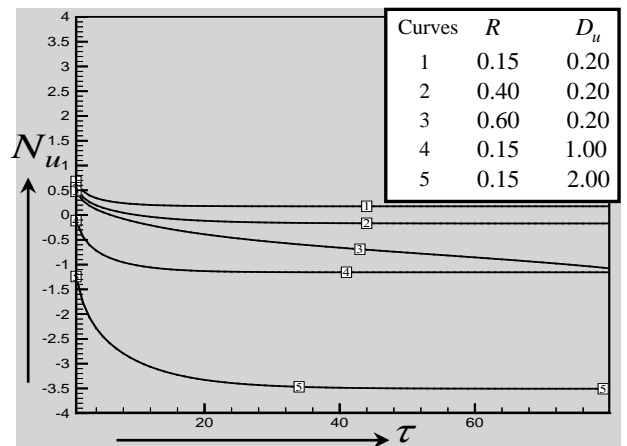

Fig.9: Nusselt number for $\varDelta$ and E_c, where $\varepsilon = 2.00$, $G_r = 1.00$, $G_m = 1.00$, $M = 1.00$, $\varLambda = 2.00$, $\lambda = 0.50$, $R = 0.15$, $P_r = 0.71$, $D_u = 0.20$, $\beta = 0.50$, $S_c = 0.60$, $S_r = 0.20$, $\gamma = 1.00$ and $S = 0.50$.

Fig.10: Nusselt number R and D_u, where $\varepsilon = 2.00$, $G_r = 1.00$, $G_m = 1.00$, $M = 1.00$, $\varDelta = 2.00$, $\varLambda = 2.00$, $\lambda = 0.50$, $P_r = 0.71$, $E_c = 0.50$, $\beta = 0.50$, $S_c = 0.60$, $S_r = 0.20$, $\gamma = 1.00$ and $S = 0.50$.
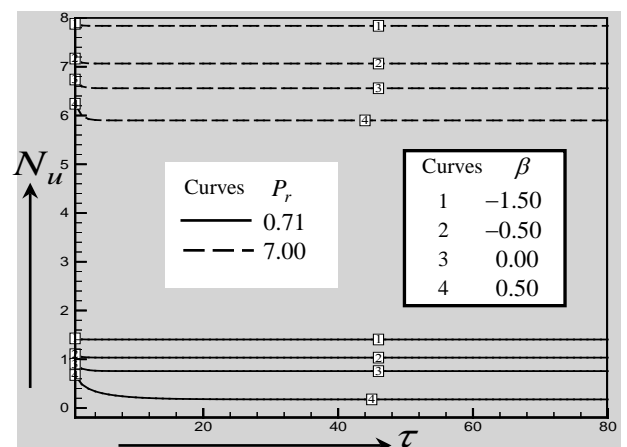

Fig.11: Nusselt number P_r and β, where $\varepsilon = 2.00$, $G_r = 1.00$, $G_m = 1.00$, $M = 1.00$, $\varDelta = 2.00$, $\varLambda = 2.00$, $\lambda = 0.50$, $R = 0.15$, $D_u = 0.20$, $E_c = 0.50$, $S_c = 0.60$, $S_r = 0.20$, $\gamma = 1.00$ and $S = 0.50$.

The effects of Suction parameter (ε) on Sherwood number have been illustrated in figure 12. It is noted that Sherwood number increases with the increase of Suction parameter. In figure 13 displays the Sherwood number for several values of Chemical reaction parameter (γ) with two values of Schimdt number $S_c = 0.60$ (water vapor) and $S_c = 0.94$ (carbon dioxide) respectively. These results show that the Sherwood number increases with the increase of Chemical reaction parameter and Schimdt number.
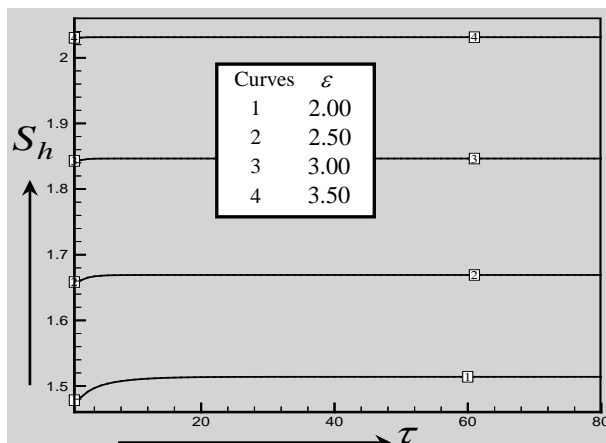

Fig.12: Sherwood number for ε, where $G_r = 1.00$, $G_m = 1.00$, $M = 1.00$, $\Delta = 2.00$, $\Lambda = 2.00$, $\lambda = 0.50$, $R = 0.15$, $P_r = 0.71$, $D_u = 0.20$, $E_c = 0.50$, $\beta = 0.50$, $S_c = 0.60$, $S_r = 0.20$, $\gamma = 1.00$ and $S = 0.50$.

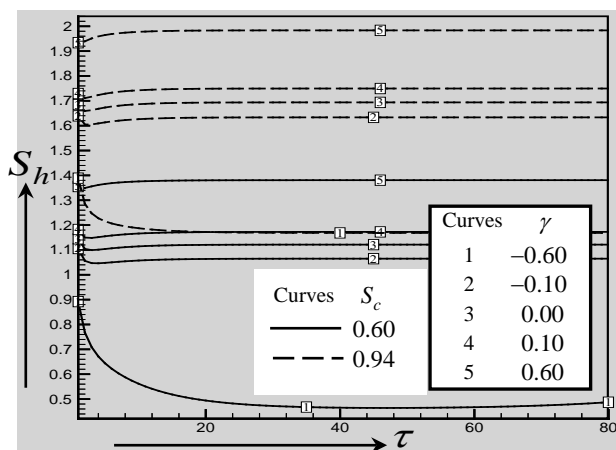Fig.13: Sherwood number S_c and γ, where $\varepsilon = 2.00$, $G_r = 1.00$, $G_m = 1.00$, $M = 1.00$, $\Delta = 2.00$, $\Lambda = 2.00$, $\lambda = 0.50$, $R = 0.15$, $P_r = 0.71$, $D_u = 0.20$, $E_c = 0.50$, $S_r = 0.20$ and $S = 0.50$.

6. CONCLUSIONS

The implicit finite difference solution of unsteady MHD chemically reacting radiative micropolar fluid flow over an impulsive vertical porous plate in the presence of heat generation, Joule heating and viscous dissipation has been studied. The physical properties are discussed for different values of parameters and compared our results with Haque and Alam's [6]. Some important findings of this investigation are listed below,

1. The shear stress increases with the increase of G_r and S_r while decreases with the increase ε and M.

2. The couple stress increases with the increase of Λ where as decreases with the increase ε and λ.

3. The Nusselt number increases with the increase of ε, Δ, and P_r while decreases with the increase of E_c, R, D_u and β.

4. The Sherwood number increases with the increase of ε, γ and S_c.

7. REFERENCES

[1] M.A. El-Haikem, A.A. Mohammadein, S.M.M. El-Kabeir, "Joule heating effects on magnetohydrodynamic free convection flow of a micropolar fluid", *International Communications in Heat and Mass Transfer*, vol. 26, no. 2, pp. 219-227, 1999.

[2] M.F. El-Amin, "Magnetohydrodynamic free convection and mass transfer flow in micropolar fluid with constant suction", *Journal of Magnetism and Magnetic Materials*, vol. 234, no. 3, pp. 567-574, 2001.

[3] M.M. Rahman, M.A. Sattar, "Magnetohydrodynamic convective flow of a micropolar fluid past a continuously moving porous plate in the presence of heat generation/absorption, *Journal of Heat Transfer*, vol. 128, no. 2, pp. 142–152, 2006.

[4] Youn J. Kim, "Heat and mass transfer in MHD micrpolar flow over a vertical moving porous plate in a porous medium", *Transport in Porous Media*, vol. 56, no. 1, pp. 17–37, 2004.

[5] Navin Kumar, Tanu Jain and Sandeep Gupta, "Effects of radiation, free convection and mass transfer on an unsteady flow of a micropolar fluid over a vertical moving porous plate immersed in a porous medium with time varying suction", *International Journal of Theoretical and Applied Science*, vol. 4, no. 1, pp. 23-29, 2012.

[6] M.M. Haque and M.M. Alam, "Soret and Joule heating effect on free convective heat generating unsteady flow of micropolar fluid through a porous medium with constant heat and mass fluxes", *Proceedings of the 13th Asian Congress of Fluid Mechanics*, Dhaka, Bangladesh, December 17-21, 2010, pp. 958-961.

[7] Carnahan B, Luther HA, Wilkes JO., 1969. Applied Numerical Methods. John Wiley and sons, New York.

8. NOMENCLATURE

Symbol	Meaning	Unit
T	Temperature	(K)
C	Concentration	(Kg/m^3)
T_w	Wall temperature	(K)
C_w	Wall concentration	(Kg/m^3)
u	Velocity component	(ms^{-1})
Ω	Angular velocity	(rad/s)
y	Cartesian Coordinate	